

Probing the potential landscape inside a two-dimensional electron-gas

J.J. Koonen*, H. Buhmann, and L.W. Molenkamp

Physikalisches Institut, Universität Würzburg, Am Hubland, 97074 Würzburg, Germany

We report direct observations of the scattering potentials in a two-dimensional electron-gas using electron-beam diffraction-experiments. The diffracting objects are local density-fluctuations caused by the spatial and charge-state distribution of the donors in the GaAs-(Al,Ga)As heterostructures. The scatterers can be manipulated externally by sample illumination, or by cooling the sample down under depleted conditions.

PACS numbers: 71.55.Eq, 72.20.Fr

The high electron mobilities that can be obtained in the two-dimensional electron-gas (2DEG) in GaAs-Al_xGa_{1-x}As heterostructures continue to fascinate the community [1,2]. At low temperatures the mobility of electrons in a perfect 2DEG is, in principle, limited by ionized donor scattering. The donors are located in the doping layer, some tens of nanometers away from the 2DEG. Due to the random distribution of donor atoms, the scattering potential is not homogeneous [3]. However, there are theoretical [4] and experimental [5,6] indications that spatial correlations between donors in different charge states reduce the ionized donor scattering and thus enhance the mobility.

These different charge states exist because for structures with a certain content of Al ($x \geq 0.2$) the electronic ground-state of the Si-donor is two-fold [7–9]: First, a shallow donor state, which is associated with a normal substitutional lattice-site and a binding energy of approximately 7 meV ($d^0 \Rightarrow d^+ + e$). Second, a more localized, deep donor level with a binding energy of ≈ 160 meV, the DX-center, which derives from lattice distortions at or near the donor site. In fact, the latter is a negatively charged donor state, DX⁻, which in contrast to the neutral and positively charged DX-states is stable with respect to the equivalent shallow donor state. At low temperatures ($T < 130$ K) DX⁻-states become stable against thermal dissociation ($DX^- \Leftrightarrow d^0 + e$).

Several aspects of the high mobilities of a 2DEG can now be explained by invoking spatial correlations between donors in different states, d⁺ and DX⁻ [5,6], where the roughening of the potential caused by donors in one state is effectively screened by donors in the other state. The electrostatic interaction should lead to regions of several tens of nanometer in diameter where all the donors are in one state [4]. These correlations lead to regions of reduced density in the 2DEG below the donors [3,4]. The correlations can be altered externally by sample illumination [8,10,11], causing a dissociation of DX⁻-centers ($E_{\text{excite}} \geq 1.2$ eV) and "bias-cooling", i.e. cooling the sample down while the 2DEG is depleted by an applied gate voltage [6,12–14] (this is an alternative to prevent the DX⁻-formation). In the experimental studies performed sofar [5,6], the mobility of a 2DEG was inferred from standard bulk conductivity measurements. Such

experiments probe an averaged scattering potential and therefore do not yield experimental information about the local distribution of shallow donors and DX-centers. Moreover, the evidence for the occurrence of donor correlations is only indirect.

In this article we use a collimated electron beam, injected and detected via quantum point-contacts (QPC), as a local probe for the scattering potentials in a 2DEG, which, as we will demonstrate, are the regions of reduced density caused by the donor state correlations. The observed interference patterns are analysed using a theoretical model based on a technique developed by M. Saito et al. [15], extended to the situation where impurities are present in the 2DEG region. This model allows for a deduction of the size and location of the scattering potentials. Experimentally, the donor configurations are changed by illumination and bias-cooling techniques.

For the experimental investigations, several gate-defined nanostructures in conventional GaAs-Al_{0.33}Ga_{0.67}As-heterojunction are used. The relevant part of the layer structure consists of 400 nm undoped GaAs, 20 nm undoped Al_{0.33}Ga_{0.67}As (spacer-layer), 38 nm 1.33×10^{18} cm⁻³ Si-doped Al_{0.33}Ga_{0.67}As, and 17 nm undoped GaAs (cap layer). Typical values for the carrier density and mobility are $n = 1.5 \dots 2.3 \times 10^{15}$ m⁻² and $\mu = 60 \dots 150$ m² (Vs)⁻¹. A schematic topview of a typical gate structure is given in Fig. 1a. Schottky-gates form two opposite QPCs (injector and detector), separated by a distance of typically $L = 4 \mu\text{m}$. In some samples the area in between the QPCs is partly covered by an additional Schottky-gate (light grey regions, Fig. 1a). The conductance of the QPC can be adjusted in such a way that only N conducting modes are transmitted ($N = G h/2e^2$). A small, low frequency ac-voltage ($V_{\text{ex}} \approx 100 \mu\text{V}$, 13 Hz) is applied to the ohmic contact I_i, injecting an electron-beam into the 2DEG. By using lock-in techniques, the voltage drop over the detector QPC is measured (contacts: V_c¹ and V_c²). Due to the smooth boundaries of an electrostatically defined QPC, the injected electron beam is collimated [16]. In a weak magnetic field perpendicular to the 2DEG plane, the electron beam is deflected by the Lorentz force.

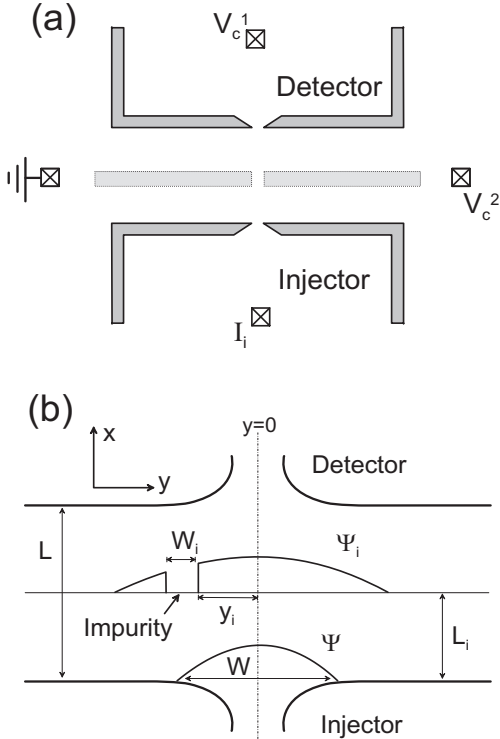


FIG. 1. Schematic view of the sample: (a) shows the gate structure and ohmic contacts (crossed squares) of the device. Dark grey: QPC gate; light grey: optional gate used for the bias-cooling experiment. (b) defines lengths and the coordinate system and displays the electron beam wavefunction Ψ at the exit of the injector quantum pointcontact (QPC) and after scattering, Ψ_i .

Therefore, the measured non-local resistance, V_c/I_i , as a function of magnetic field provides information about the beam profile. Experimentally, the measured beam profile is not smooth, but rather exhibits additional structure (see Fig. 2, 3, 4, and Fig. 1 Ref. [16]). Also other groups [17,18] presented data exhibiting these features, but their origin has not been discussed previously.

In the experiments, the samples were cooled down to 1.8 K and the QPC transmittance was adjusted to $N = 1$ for injector and detector. Figures 2, 3 and 4 show typical examples of measured non-local magnetoresistances. The observed structures are attributed to electron interference effects because of its marked temperature dependence (cf. Fig. 2). The interference patterns are stable in time and characteristic for a given sample and a given cooling cycle. Between different cooling cycles the interference pattern changes only slightly. This is in strong contrast with typical observations on electronic quantum interferences, e.g. universal conductance fluctuations (UCF). UCF are related to electron scattering with single impurities, whose 'fingerprint' varies strongly from cooldown to cooldown, while, as discussed in the introduction, in high-mobility 2DEGs scattering is due to random potential fluctuations, which depend on the much more robust spatial charge correlations of donors.

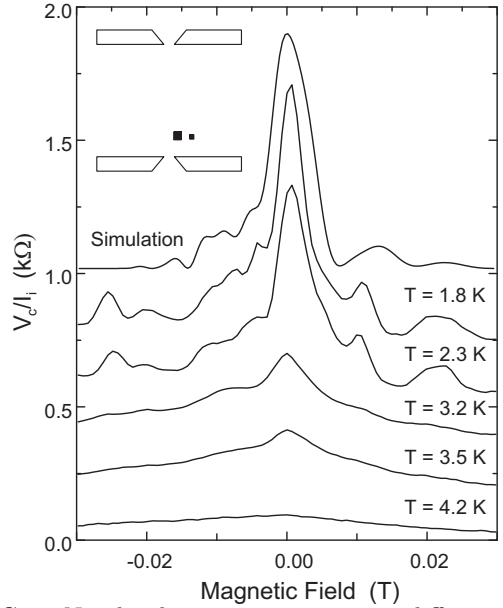


FIG. 2. Non-local magnetoresistance at different temperature. A simulation of the experimental result (at 1.8 K) is obtained for a scatterer configuration indicated schematically in the top left corner: $L_{i,1} = 0.6 \mu\text{m}$, $0.1 \leq y_i \leq 0.2 \mu\text{m}$ and $L_{i,2} = 0.6 \mu\text{m}$, $0.4 \leq y_i \leq 0.42 \mu\text{m}$.

In order to substantiate our interpretation of the experimental observations it is now necessary to model the experimentally found diffraction patterns to gain information about size and location of scattering potentials. We use the simplest possible model, based on an extension of the method of Saito et al. [15]. The electron wavefunction at the exit of a QPC can be written as

$$\Psi_0(0, y) = \left(\frac{2}{W} \right)^{1/2} \cos \left(\frac{\pi y}{W} \right) \text{ for } -W/2 \leq y \leq W/2, \quad (1)$$

and zero elsewhere, if the QPC carries only one conducting mode (cf. Fig. 1b). W denotes the point-contact width at the exit. Using Green's theorem with Dirichlet's boundary conditions the wavefunction can be calculated for any point of the half-plane ($x > 0$):

$$\Psi(\mathbf{r}') = \frac{i}{2m^*} \int_S dS \mathbf{n}(\mathbf{r}) \cdot [\Psi(\mathbf{r}) (-i\hbar \nabla_{\mathbf{r}}) G^+(\mathbf{r}', \mathbf{r})]. \quad (2)$$

G^+ , the Green's function in a weak magnetic field, which can be approximated by the Green's function at zero field, $G^0(\mathbf{r}', \mathbf{r})$, and a phase factor, $\theta(\mathbf{r}', \mathbf{r})$:

$$G^+(\mathbf{r}', \mathbf{r}) \simeq e^{i\theta(\mathbf{r}', \mathbf{r})} G^0(\mathbf{r}', \mathbf{r}), \quad (3)$$

$$\theta(\mathbf{r}', \mathbf{r}) = -\frac{e}{\hbar} \int \mathbf{A}(\mathbf{R}(t)) \cdot \frac{\nabla_{\mathbf{R}} G^0(\mathbf{R}(t), \mathbf{r})}{|\nabla_{\mathbf{R}} G^0(\mathbf{R}(t), \mathbf{r})|} dt, \quad (4)$$

a line-integral along the gradient of $G^0(\mathbf{r}', \mathbf{r})$. For a detailed description of this method we refer to Ref. [15].

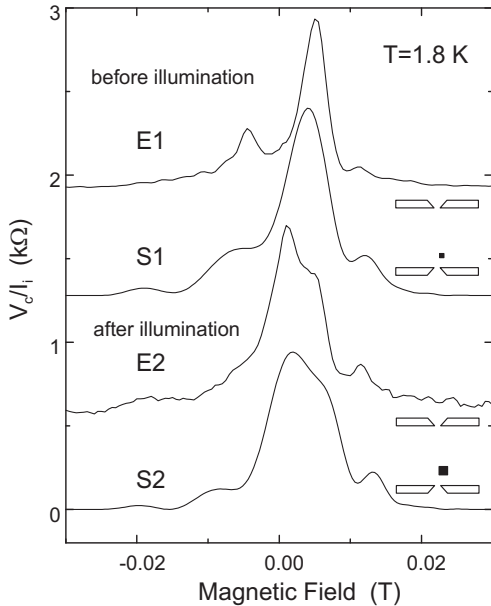


FIG. 3. Experiment (E) and simulation (S) of the collimation signal before (1) and after illumination (2). The fit parameter for traces S1 and S2 are: $L_i = 0.65 \mu\text{m}$, $0.08 \leq y_i \leq 0.16 \mu\text{m}$ and $L_i = 0.65 \mu\text{m}$, $0.08 \leq y_i \leq 0.22 \mu\text{m}$, respectively.

The wavefunction in the detector QPC, $\Psi_D(L, y)$, at a distance $x = L$ can be written analogous to Eq. 1 (for one conducting mode). Thus, the transmission coefficient from the injector to the detector QPC can be calculated:

$$T = \left| \int_{-W/2}^{W/2} \Psi_D^*(l, y') \Psi(l, y') dy' \right|^2. \quad (5)$$

In order to simulate impurities, an intermediate line is introduced between injector and detector QPC, ($0 < x = L_i < L$). The wavefunction Ψ_i is calculated at this line. The simplest model for the effect of a scattering object on the electronic wavefunction is just to set a part of the wavefunction Ψ_i to zero, schematically shown in Fig. 1b. This modified wavefunction is then propagated further to calculate the detector wavefunction Ψ_D ; Eq. 5 then gives the transmission probability. Of course, cutting off parts of a wavefunction is a very crude method to simulate scattering. Neither diffusive back- or forward-scattering nor wavefunction matching at the boundaries are considered. However, a comparison with the experiment shows that this model yields a reasonable reproduction of the main features of the observed interference patterns (see Fig. 2).

From fitting the theoretical curves to the experimental traces it is possible to deduce values for the distance L_i and the width W_i of scattering potential, yielding two scattering centers for the example displayed in Fig. 2: $L_{i,1} = 0.6 \mu\text{m}$, $W_{i,1} = 0.1 \mu\text{m}$ ($0.1 \leq y_i \leq 0.2 \mu\text{m}$) and $L_{i,2} = 0.6 \mu\text{m}$, $W_{i,2} = 0.02 \mu\text{m}$ ($0.4 \leq y_i \leq 0.42 \mu\text{m}$). The configuration of the scattering objects is schematically shown in the inset of Fig. 2. Already small variation

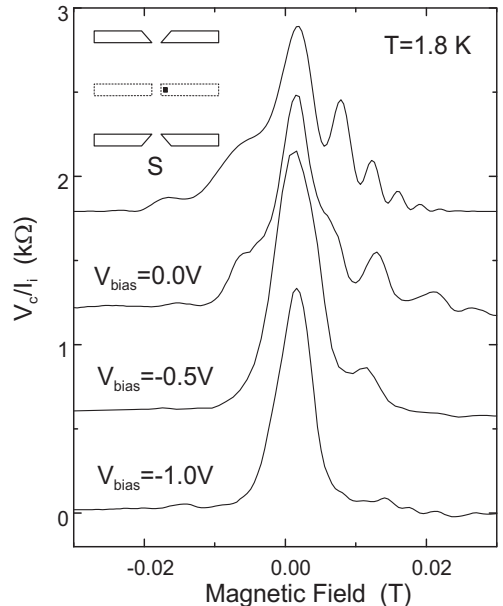


FIG. 4. Experiment and simulation (S) of the collimation signal for the bias-cooling experiment. The applied voltages are indicated in the figure. The fit parameter for trace S is: $L_i = 2.00 \mu\text{m}$ and $0.18 \leq y_i \leq 0.23 \mu\text{m}$.

of the size or location has a drastic effect on the observed interference patterns. From comparing the numerical results we estimate the uncertainty of the fitted values for L_i and W_i as less than 5%.

Now experiments were done to prove that the diffracting objects are due to correlations in the distribution of donor states. Fig. 3, trace E1, shows the observed interference pattern for a sample cooled down in the dark. At 1.8 K the QPCs were defined and the collimation signal was measured. The simulation yielded a width of $W_{i,S1} = 0.08 \mu\text{m}$ in a distance $L_{i,S1} = 0.65 \mu\text{m}$. Subsequently, the device was illuminated using a $100 \mu\text{s}$ light pulse of a red light-emitting diode ($\lambda = 670 \text{ nm}$) close to the sample. The resulting interference pattern differs significantly from the initial (Fig. 3, trace E2). Within the model for DX-center formation described above, this change can be attributed to a light induced transformation of donors in the DX^- -state into the d^+ -state. At the same time the sample exhibits a slight increase in the carrier density, in good agreement with a $\text{DX}^- \rightarrow \text{d}^+$ conversion. From the simulation S2 an increase in the width of the scattering potential is found ($W_{i,S2} = 0.14 \mu\text{m}$). The observed change in the interference pattern of the electron beam is direct evidence for a reconfiguration of the scattering potential in the vicinity of the electron beam.

In Fig. 4 experimental curves are shown for a sample with an extra pair of gates between injector and detector. As indicated in Fig. 1a, these intermediate gates have a small gap of approximate 300 nm centered at the line connecting injector and detector. The collimation

signal of this sample, cooled down without the intermediate gates defined, exhibits a distinct interference pattern. The simulation S reveals a scattering potential in the vicinity of the electron beam just underneath the intermediate gate ($L_i = 2.00 \mu\text{m}$ and $0.18 \leq y_i \leq 0.23 \mu\text{m}$) for $V_{\text{bias}} = 0 \text{ V}$). As demonstrated in Ref. [6] one may suppress the formation of DX-centers by depleting the 2DEG through the application of a negative bias voltage at high temperatures. Below $T = 130 \text{ K}$ this (uncorrelated) donor configuration will be stable against thermal activation and the bias voltage can be released. The interference patterns resulting from applying exactly this procedure to intermediate gates are shown in Fig. 4 for $V_{\text{bias}} = 0.0, -0.5$ and -1.0 V . The initial interferences are suppressed with increasing negative bias voltage. This can be understood by considering that the applied bias voltage suppresses the formation of DX^- -Centers underneath the gates, leading to a smoothening of the potential landscape in these regions.

A common result of all simulations is that the size of the scattering potential is in the order of 50 to 150 nm, comparable to those found in selfconsistent calculations for the size of potential fluctuations in a 2DEG due to a random distribution of correlated donors [3,4]. It is therefore very likely that the observed interference effects are related to donor complexes. Additional evidence for this conclusion is that modifying the distribution of charged donors by illumination or bias-cooling immediately effects the observed electron-beam interferences.

In conclusion, electron-beam experiments probe directly the existance of long range correlations between donors in GaAs-(Al,Ga)As heterostructure on a microscopic level. We used a numerical methode to simulate scattering potentials in the path of the electron beam in 2DEG layer. It was possible to deduce the position and size of actual scattering potentials by fitting experimentally obtained interference pattern of an electron-beam signal. The typical size of the scatterers (50...150 nm) implies a collective effect of randomly distributed donors. This distribution could be changed by reducing the number of DX^- -centers through illumination and bias-cooling techniques. The experiments show that a collimated electron beam is a sensitive tool in the investigation of local potential fluctuations in a 2DEG. It would be of interest to develop a more sophisticated theory of electron-beam scattering. Simulations using such a theory could in combination with e.g. density-dependent experiments on the interference structures be used to yield a detailed picture of the shape and size of the density fluctuations in a 2DEG.

ACKNOWLEDGMENTS

The authers thank A.R. Long for discussions. Part of this work was supported by the DFG under MO 771/1-1 and MO 771/3-1, and by the Volkswagen Stiftung.

* Delft University of Technology, Department of Applied Physics, 2600 GA Delft, The Netherlands.

- [1] T. Saku, Y. Horikoshi, and Y. Tokura, *Jpn. J. Appl. Phys.* **35**, 34 (1996).
- [2] V. Umansky, R. de-Picciotto, and M. Heiblum, *Appl. Phys. Lett.* **71**, 683 (1997).
- [3] J. A. Nixon and J. H. Davies, *Phys. Rev. B* **41**, (1990).
- [4] A. L. Efros, F. G. Pikus, and G. G. Samsonidze, *Phys. Rev. B* **41**, 8295 (1990).
- [5] P. T. Coleridge, *Phys. Rev. B* **44**, 3793 (1991).
- [6] E. Buks, M. Heiblum, and H. Shtrikman, *Phys. Rev. B* **49**, 14790 (1994).
- [7] H. J. Queisser and E. E. Haller, *Science* **281** 945 (1998).
- [8] D. J. Chadi and K. J. Chang, *Phys. Rev. B* **39**, 10063 (1989).
- [9] S. Bednarek and J. Adamowski, *Phys. Rev. B* **55**, (1997).
- [10] R. Fletcher, E. Zaremba, M. D'Iorio, C. T. Foxon, and J. J. Harris, *Phys. Rev. B* **41**, (1990).
- [11] M. Hayne, A. Usher, J. J. Harris, V. V. Moshchalkov, and C. T. Foxon, *Phys. Rev. B* **57**, 14813 (1998).
- [12] A. R. Long, J. H. Davies, M. Kinsler, S. Vallis, and M. C. Holland, *Semicond. Sci. Technol.* **8**, 1581 (1993).
- [13] E. Skuras, M. C. Holland, C. J. Barton, J. H. Davies, and A. R. Long, *Semicond. Sci. Technol.* **10**, 922 (1995).
- [14] P. T. Coleridge, *Semicond. Sci. Technol.* **12**, 22 (1997).
- [15] M. Saito, M. Takatsu, M. Okada, and N. Yokoyama, *Phys. Rev. B* **46**, 13220 (1992).
- [16] L. W. Molenkamp, A. A. M. Staring, C. W. J. Beenakker, R. Eppenga, C. E. Timmering, J. G. Williams, C. J. P. M. Harmans, and C. T. Foxon, *Phys. Rev. B* **41**, 1274 (1990).
- [17] M. Okada, M. Saito, M. Takatsu, K. Kosemura, T. Nagata, H. Ishiwari, and N. Yokoyama, *Superlatt. Microstruct.* **10**, 493 (1991). These authors report on a splitting in the electron beam signal which is attributed to diffraction of the beam at the QPC exit. However, as shown in [16], the QPC potential is smooth. Based on the results reported here, we suggest that the observations Okada et al. have a similar origin as the diffraction patterns discussed in the present paper.
- [18] K. L. Shepard, M. L. Roukes, and B. P. van der Gaag, *Phys. Rev. B* **46**, 9648 (1992). J. Appenzeller, *Berichte des Forschungszentrums Jülich*, JüL-3080 (1995); G. Timp, *Semiconductors and Semimetals* Vol. **35**, ed. M. Reed, Academic Press 1992, p. 113 pp.